Effect of nano-scale precipitation on strengthening of ferritic ODS Fe-Cr-Al alloy

C. Capdevila[1], J. Chao[1], J.A. Jimenez[1] and M. K. Miller[2]

[1]Centro Nacional de Investigaciones Metalúrgicas (CENIM-CSIC),

Avda. Gregorio del Amo, 8, 28040 Madrid, Spain

[2] Materials Science and Technology Division, Oak Ridge National Laboratory,

PO Box 2008, Oak Ridge, TN 37831-6136, USA

Abstract

The kinetics of Fe-rich (α) and Cr-rich (α') phase separation during ageing of Fe-Cr-Al oxide dispersion strengthened (ODS) alloys have been analyzed with a combination of atom probe tomography (APT) and thermoelectric power (TEP) measurements. The slight lattice parameter decrease measured by X-ray diffraction after thermal ageing was associated with a lattice misfit between the emerging α and α' domains. The elastic strain associated to this misfit and the different elastic modulus for the α and α' phases would produce an increase in internal stresses that would retard the motion of dislocations and thus would be the main cause for the strengthening.

Keywords: phase separation, ferrous alloy, mechanical alloying, tomography, thermoelectric power, spinodal decomposition

Introduction

The oxide dispersion strengthened (ODS) Fe-Cr ferritic steels, in both coarse- and fine-grained microstructure conditions, have been developed to be used at elevated temperatures due to their excellent high-temperature creep strength and good oxidation resistance. The presence of extremely thermally stable oxide particle evenly dispersed within the ferritic matrix allows the strength to be maintained up to much higher temperatures than conventional alloys. The development of ODS ferritic alloys has been conducted in the fields of fast reactor fuel cladding applications [1] and fusion reactor materials applications [2-3]. However, these alloys face a severe hardening and embritlement problem because their service temperature lies in the range of 300-500 °C. This embritlement, known for decades as "475°C embritlement" of the high Cr ferritic steels, is related to the microstructural decomposition of the ferrite in Fe-rich (α) and Cr-rich (α') phases. Since the formation of a Cr-rich α ´ phase results in an increase of yield and tensile strength, and a reduction in ductility, the response of the material in service is partly determined by the ferrite decomposition, that will inevitably undergo after prolonged service times. As limited data are available for the microstructural and mechanical property changes of high Cr ODS steels after thermal ageing treatments, these steels are at the centre of much basic research, both experimental and numerical [4-6]. The goal of this paper is to study the α -α' phase separation process occurring in the temperature range of 300 – 500 °C on a commercial PM 2000™ ODS alloy and to determine the effect of this decomposition process on the strengthening of the material. This study will include the monitorization of the α - α' phase separation kinetics by APT and TEP and the changes induced in lattice parameter by X-ray diffraction.

Materials and Experimental Procedure

The PM 2000™ ODS alloy used in this study was commercially manufactured by Plansee GmbH. This alloy is a dispersion-strengthened steel manufactured by a mechanical alloying (MA) process in a hydrogen

atmosphere, as described elsewhere [7]. The composition of the alloy (in at. %) was 18.5 % Cr, 10.5% Al, 0.58% Ti, 0.23% Y, 0.28% O, 0.17% C and 0.022% N.

Needle-shaped specimens for APT were cut from the bulk material and electropolished with the use of the standard double layer and micropolishing methods [8]. Atom probe tomography analyses were performed with a Cameca Instruments LEAP 2017 local electrode atom probe (LEAP®) which was operated in voltage-pulsed mode with a specimen temperature of 60 K, a pulse repetition rate of 200 kHz, and a pulse fraction of 0.2.

The set-up of the TEP equipment is given elsewhere [9]. For this technique, the sample is held between two blocks of a reference metal (99.999% pure iron in this case), between which a temperature difference ΔT=10 K is applied. The apparatus measures the relative TEP (ΔS) of the sample in comparison to the TEP of pure iron at 20 K. The resolution of the equipment is 1 nV/K.

Room temperature tensile tests were carried out in an universal testing machine at a strain rate of 10^{-4} s^{-1} in samples with a gauge length of 45 mm and a diameter of 8 mm. A Class B1 extensometer with a gage length of 40 mm was used to measure the elongation. The main mechanical properties, such as Young's modulus (E), 0.2% yield strength (YS), ultimate tensile strength (UTS), and tensile elongation, were evaluated from the engineering stress/strain curves. E values were obtained from the stress-strain curve. The slope of the linear elastic region of the curve should nominally correspond to the Young's Modulus of the material being tested. However, a measurement of Modulus from a standard tensile test can lead to non-accurate values, since any slight misalignment of the loading train and the test piece can result in gross errors of the apparent modulus measurement. In order to obtain reasonably accurate measurement, an average value of the modulus was determined from 20 individual measurements. Each measurement consisted of attaching the extensometer to the specimen, loading the specimen to 60% of the yield strength, unloading the specimen, and removing the extensometer.

X ray diffraction measurements were carried out with a Bruker AXS D8 diffractometer equipped with X-ray Co tube and Goebel mirror optics to obtain a parallel and monochromatic X-ray beam. Operational conditions were selected to obtain the desired statistical accuracy. It is well known that the Rietveld

method is a powerful tool for calculation of structural parameters like the lattice parameters from diffraction patterns. In this study, we have used the version 4.0 of Rietveld analysis program TOPAS (Bruker AXS) for the XRD data refinement. Beside the unit cell parameter, the refinement protocol included also the background, zero displacement, the scale factors, the peak breath and texture parameters. The lattice parameters are determined with an accuracy of 0.0001 nm

Results and discussion

Microstructure of PM 2000

Immediately after the MA process, the powders have a grain size, which can be as fine as 1±2 nm locally [10]. This is hardly surprising given the extent of the deformation during MA, with true strains of the order of ε = 9, equivalent to stretching a unit length by a factor of 8000. The consolidation process involves hot extrusion and rolling at ~1000 °C. It is known that during the course of consolidation, the material may dynamically recrystallize several times [11-12], which leads to the formation of elongated grains that are slightly longer in the longitudinal direction (average of 1.5 μm in length in the longitudinal direction by ~0.5 μm in diameter in the transversal direction). The material exhibits a weak <110> fiber texture. Subsequent heat treatment at a temperature close to 0.75 the melting temperature (1100 °C for 100 h) leads to the formation of an equiaxed coarser grained microstructure with a grain average size of ~2 μm [11], in spite of the strong alignment of the aluminum-yttrium oxide particles along the extrusion direction [13-14]. Previous research [15] revealed the thermal stability of such oxide particles, which have an average diameter of 20 nm after this recrystallization heat treatment. However, these oxide particles are one order of magnitude larger than the expected size of α′ particles according to literature [16].

The α-α′ phase separation kinetics

Phase separation within the low-temperature miscibility gap occurred in the PM 2000 alloy during the isothermal holding at temperatures ranging from 400 to 475 °C to form Fe-rich α and Cr-enriched α′ phases [17]. The fine scale microstructure for selected ageing temperatures and times is studied by means of atom

maps as in the example shown in Figure 1(a). Decomposition into Cr-enriched α' and Cr-depleted α regions is clearly shown after ageing for 2000 h at 475 °C. Besides the Cr-rich precipitates, the presence of Al- and Ti- enriched precipitates was also recorded during APT analysis, as shown in Figure 1(b), although these particles were present in a significantly lower number density compared to the Cr-rich nanoprecipitates forming the α' phase. This Al- and Ti-enriched phase corresponds to the B2-ordered FeAl (β') phase with the Ti substituting for the Al (as it does in Ni_3Al). This B2 phase is also the basis of several iron-based superalloys (Fe-Al-Ni-Mo) that were shown to have an approximate composition of 51% Al, 38% Ni, and 11% Fe [18].

The three-dimensional microstructure, as determined by APT, resulting from ageing at 475 °C, is shown in Figure 2. Because of the relatively low chromium content of the alloy, the Cr-rich α' phase is in the form of isolated particles rather than the interconnected network structure observed previously in Fe-24-45% Cr alloys [19]. The kinetics of the α-α' phase separation were quantitatively determined by analyzing the evolution of the Cr-content of α' nanoparticles ($C_{Cr}^{\alpha'}$). The value of $C_{Cr}^{\alpha'}$ was determined from the proximity histograms [20]. The evolution of the ratio (ξ) between $C_{Cr}^{\alpha'}$ and the α' phase composition was determined by the phase diagram, which will indicate the extent of the α-α' phase separation at 400, 435 and 475 °C with time, and is shown in Figure 3(a). It is clear that the higher the ageing temperature, the faster the phase separation kinetics.

The analysis of phase compositions from proximity histograms also revealed the Al-partitioning between the matrix and α' phase. The variation of the Al-partitioning factor ($k_{Al} = [Al]_{\alpha} / [Al]_{\alpha'}$) with composition amplitude of α-α' phase separation (ΔC_{Cr}) during ageing at temperatures ranging from 400 to 475 °C is shown in Figure 3(b). It could be concluded that Al-partitioning will occur at all the ageing temperatures tested, and the lack of evidence at low ageing temperatures, i.e., 400 °C, is a consequence of the slow α-α' phase separation kinetics at this temperature [21].

The α-α' phase separation kinetics observed by APT were confirmed with an alternative experimental technique, TEP, which is used to analyze significantly greater volumes than possible in the APT needle-shaped samples. The TEP measurement (ΔS) evolution with ageing time at temperatures ranging from 400

to 475 °C is governed by two effects [22], as shown in Figure 4(a). The first effect is attributed to the gradual decrease of the solute content (i.e., Cr) in the matrix as phase separation proceeds. This contribution is generally divided into two terms: a diffusion component and a phonon drag component. The first term is usually taken as a linear function of temperature and includes the solute content. The second term depends on the electron and phonon scattering processes. Solute atoms can have a positive or negative influence on the TEP of the matrix. In particular, it is known that solutes decrease the TEP of iron [23]. The second effect is ascribed to the intrinsic effect of the precipitates formed during ageing. This effect depends on the volume fraction, type, size, and morphology of the precipitates [22]. It has been reported that a low volume fraction (below 10%) of coarse, incoherent precipitates has a negligible influence on the TEP, whereas coherent and semi-coherent precipitates, such as the α′ phase in this work, may have a strong intrinsic effect on the TEP of the alloy. The fraction of α′ phase precipitated could be related to the TEP values by defining the ratio Y as follows:

$$Y = \frac{\Delta S_t - \Delta S_i}{\Delta S_f - \Delta S_i}, \quad (1)$$

where ΔS_t is the relative power measurement obtained for a time t, ΔS_f and ΔS_i are the relative power measurement obtained at the stabilization level shown in Figure 4(a) and the initial stage, respectively.

A detailed analysis of α'-phase precipitation kinetics can be obtained from the direct fit of the TEP data to the Austin-Rickett (AR) relationship [24]. From this analysis, kinetic parameters, such as the so-called Avrami exponent and the activation energy, can be calculated to provide significant understanding of the nucleation and growth process of the α' nanoprecipitates [17]. Therefore, the TEP could be adapted to an AR equation assuming that $\ln Y \sim k(T) \times t^n$. The temperature dependent factor k(T) follows an Arrhenius type expression such as $k(T) = k_0 \exp(-Q/RT)$, where R is the gas constant, T the absolute temperature, and Q the activation energy for the process. The evolution of ln(Y/(1-Y)) vs. ln t is shown in Figure 4(b). It can be concluded from Figure 4(c) that the Q value for α-α′ phase separation in PM 2000 is 264 kJ mol^{-1}. This value is consistent with the activation energy for self-diffusion of Cr in α-Fe, which is 248 kJ mol^{-1} [25]. This fit indicates an average value of n = 1.2, which is close to the ideal 1.5 value that in accordance with Starink

[26], describes a three-dimensional, homogeneous nucleation with a very low nucleation rate. Therefore, the α-α′ phase separation process in PM 2000 can be described as particles growing in three dimensions starting from small sizes, with a growth rate controlled by volume diffusion (of Cr) and a decreasing nucleation rate. This conclusion is consistent with the APT results presented above, which indicate a transient coarsening mechanism, i.e., an overlap between nucleation, growth, and coarsening that occurs because of the very low α-α′ interfacial energy and substantial supersaturation of Cr in the matrix.

Effect of phase separation on lattice parameter of PM2000

The evolution of the ferrite lattice parameter (a) with ageing time at 475 °C is shown in Figure 5(a). In this figure, it is observed a decrease of the lattice parameter from 0.2890 ± 0.0001 nm in the unaged condition to 0.2885 ± 0.0001 nm after ageing for 2000 h at 475 °C. The reason for such a decrease can be related with to the structure of the unstable ferrite evolving during phase separation. Ferrite decomposes into two phases with favorable atomic bonding configurations (i.e., Fe-Fe and Cr-Cr bonds), leading to a more deeply compacted ferrite phase, as reported elsewhere [11]. The decrease in lattice parameter as the α -α' phase separation progress is clearly shown in Figure 5(b).

Mechanical properties evolution during ferrite decomposition

Values of the main tensile properties measured at room temperature as a function of ageing time at 475°C are summarized in Table 1. As the ageing time increases, it is observed a progressive increase of the E, 0.2% yield strength, and tensile strength tensile with increasing the time of ageing. Based on these results, it was concluded that the presence of α' domains in ODS steels hinders the motion of dislocations and hardens the materials, which results in the loss of ductility shown in this table.

Macroscopic elastic strain has its origin in the forces between the atoms of the solid, and therefore depends on both the nature of chemical bonding and the inter-atomic distance. As a consequence, the magnitude of E is a measure of the resistance to separation of adjacent atoms, e.g., the interatomic bonding forces. Since the inter-atomic forces will strongly depend on the inter-atomic distance, E should to some extent be related to the lattice parameter. Therefore, a decrease in lattice parameter, as the one reported above during α-α' phase separation, would lead to shrinkage similar to that caused by a change in

hydrostatic pressure ΔP. The pressure and dilatation ($\Delta V/V$) are related to the bulk modulus (K) by the following equation [27]:

$$\Delta P = K\frac{\Delta V}{V} \quad (2)$$

Assuming that for a Poisson's ratio of ν = 0.33 for α-Fe and K and E are related by $K = E/3(1-2\nu)$, the change in volume for a cubic crystal could be approximated by $\Delta V/V \sim 3\Delta a/a$ where a represents the lattice parameter, ΔP could be approximated as:

$$\Delta P \approx 3\frac{a^{0h} - a^{500h}}{a^{500h}} E_{500h} \quad (3)$$

The above expression would give a sensible approach to estimate the change in pressure associated with the change of lattice parameter reported above from the unaged condition (a^{0h}) to that after ageing for 500 h (a^{500h}) and from a value of E at unaged condition to E_{500h}=190 GPa (Table 1). Introducing in equation (3) the values of a^{0h} and a^{500h} represented in Figure 6, it is deduced a value of $\Delta P \sim 4$ GPa.

The Grüneisen parameter for α-Fe is $\gamma \sim 1.7$ [28]. On account of the expression

$$\gamma = \frac{1}{2}\left(\frac{\partial K}{\partial P} - 1\right), \quad (4)$$

where K is the bulk modulus, and P is the pressure, introducing the value of ΔP calculated above a results in a increase in the Young's modulus of $\Delta E \sim 18$ GPa. As shown in Table 1, this value is consistent with the increases in E from the unaged condition to the one recorded after ageing at 500 h.

Hence, it could be concluded that the more compacted microstructure associated with the α-α' phase separation process is directly associated with the observed decrease of the PM 2000 lattice parameter, and this lattice parameter decrease will be related to the Young's modulus increase with ageing time measured. On the other hand, the effect of B2 precipitation is negligible since it does not remove enough aluminum from the α phase to produce a change in the lattice parameter of the ferrite.

Hardening mechanism during α′ phase nanoprecipitation

The evolution of the increment of yield strength (ΔYS) with ΔC_{Cr} is shown in Figure 6. The strength increases almost proportionally with the amplitude of the Cr concentration in the α′ phase, which indicates that the strengthening mechanism is closely related to the α-α′ phase separation process. The effect of the phase separation process on strengthening is twofold: firstly, the α-α′ phase separation induces a stress field (misfit between the α and α′ phases) that hinders dislocations from propagating, as described by Cahn [29]. Cahn also reported that a dislocation in a phase separated structure experiences a force from the internal stresses due to periodic variations of the lattice parameter. Secondly, the spatial variation in the Young's modulus associated with the composition modulation is also considered as an obstacle for the motion of dislocations. Previous work on the strain hardening of an Fe-30% Cr alloy [30] showed that the above two factors contribute to the major fraction of the increment of YS and constitute the athermal component of the increment of yield strength [30]. It was also proposed that the thermal component of the increment of yield strength can be attributed to the increase of the retarding force of Fe-Cr bonds on the dislocation movement relative to those of Fe-Fe and Cr-Cr bonds [30].

Conclusions

The combined results from APT and TEP measurements suggest that the α-α′ phase separation process in PM 2000 can be described as particles growing in three dimensions starting from small sizes, with a growth rate controlled by volume diffusion (of Cr) and a decreasing nucleation rate. This conclusion is consistent with the APT results presented, which indicate a transient coarsening mechanism, i.e., an overlap between nucleation, growth, and coarsening occurs because of the very low α-α′ interfacial energy and substantial supersaturation of Cr in the matrix. Likewise, the APT proximity histogram analysis revealed significant partitioning of the aluminum to the Fe-rich α phase during isothermal ageing at 435 and 475 °C for times between 10 and 3600 h, but Al partitioning is negligible at 400 °C after ageing for 3600 h.

The comparison between APT and X-ray diffraction results indicate that the detected decrease in lattice parameter is a direct consequence of α-α' phase separation, which results in a more compacted structure. The decrease in lattice parameter leads to progressive Young's modulus increase during α-α' phase separation by ageing at intermediate temperatures. This fact, along with the linear relationship observed between the incremental change of yield strength and ΔC_{Cr}, indicates that the strengthening induced by the the presence of α' domains in PM 2000 can be explained by the athermal components of the yield strength (i.e. stress field induced by the misfit between α and α' phases, and the modulus effect).

Acknowledgements

PM 2000™ is a trademark of Plansee GmbH. LEAP® is a registered trademark of Cameca Instruments. Authors acknowledge financial support to Spanish Ministerio de Ciencia e Innovación through in the form of a Coordinate Project in the Energy Area of Plan Nacional 2009 (ENE2009-13766-C04-01). Research supported by ORNL's Shared Research Equipment (ShaRE) User Facility, which is sponsored by the Office of Basic Energy Sciences, U.S. Department of Energy.

References

[1]. S. Ukai, M. Harada, H. Okada, M. Inoue, S. Nomura, S. Shikakura, K. Asabe, T. Nishida, M. Fujiwara, J. Nucl. Mater. 204 (1993) 65.

[2]. M.K. Miller, K.F. Russell, J. Nuc. Mater. 371 (2007) 145.

[3]. P. Pareige, M.K. Miller, R.E. Stoller, D.T. Hoelzer, E. Cadel, B. Radiguet, J. Nuc. Mater. 360 (2007) 136.

[4]. G. Bonny, D. Terentyev, L. Malerba, J. Phase Equilib. Diff. 31 (2010) 439.

[5]. S. Novy, P. Pareige, C. Pareige, J. Nuc. Mater. 384 (2009) 96.

[6]. C. Pareige, M. Roussel, S. Novy, V. Kuksenko, P. Olsson, C. Domain, P. Pareige, Acta Mater. 59 (2011) 2404.

[7]. C. Capdevila, Y. L. Chen, N. C. K. Lassen, A. R. Jones, H. K. D. H. Bhadeshia, Mat. Sci. Technol. 17 (2001) 693.

[8]. M. K. Miller, Atom Probe Tomography, Kluwer Academic/Plenum Press, New York, NY, 2000.

[9]. F. G. Caballero, C. Capdevila, L. F. Alvarez and C. Garcia de Andres, Scr. Mater. 50 (2004) 1061.

[10]. C. Capdevila, U. Miller, H. Jelenak, H. K. D. H. Bhadeshia, Mater. Sci. Eng. A 316 (2001) 161.

[11]. C. Capdevila, MK Miller, I. Toda, J. Chao, Mater. Sci. Eng. A 527 (2010) 7931.

[12]. J.L. Gonzalez-Carrasco, J. Chao, C. Capdevila, J.A. Jimenez, V. Amigo, M.D. Salvador, Mater. Sci. Eng. A 471 (2007) 120.

[13]. C. Capdevila, H. K. D. H. Bhadeshia, Adv. Eng. Mater. 3 (2001) 647.

[14]. C.C. Montes, H. K. D. H. Bhadeshia, Adv. Eng. Mater. 5 (2003) 232.

[15]. C. Capdevila, Metall. Mater. Trans. A 36 (2005) 1547.

[16]. M.K. Miller, J.M. Hyde, A. Cerezo, G.D.W. Smith, Appl. Surf. Sci. 87-88 (1995) 323.

[17]. C. Capdevila, M.K. Miller, J. Chao, Acta Mater. 60 (2012) 4673.

[18]. M. K. Miller, J. M. Hyde, M. G. Hetherington, A. Cerezo, G. D. W. Smith, C. M. Elliott, Acta Metall. Mater. 43 (1995) 3385.

[19]. M. K. Miller, M. G. Hetherington, J. R. Weertman, H. A. Calderon, in: G. M. Stocks, D. P. Pope, A. F. Giamei (Eds.), Alloy Phase Stability and Design, MRS Publishing, Pittsburgh, PA, 1991, p. 219.

[20]. O. C. Hellman, J. A. Vandenbroucke, J. Rüsing, D. Isheim, D. N. Seidman, Microsc. Microanal. 6 (2000) 437.

[21]. C. Capdevila, M.K. Miller, G. Pimentel, J. Chao, Scr. Mater. 66 (2012) 254.

[22]. J. M. Pelletier, R. Borrelly, Mater. Sci. Eng. 55 (1982) 191.

[23]. A. Brahmi, R. Borrelly, Acta Mater. 45 (1997) 1889.

[24]. J.B. Austin, R.L Rickett, Trans Am Inst Met Eng 135 (1939) 396.

[25]. H.W. Paxton, T. Kunitake, Trans. Metall. Soc. AIME 218 (1960) 1003.

[26]. J.W. Christian. The theory of transformations in metals and alloys. Part I: equilibium and general kinetics theory, vol 1. Oxford: Pergamon Press, 1981.

[27]. M. F. Ashby, D. R. H. Jones: Engineering Materials, 2nd edition, Butterworth – Heinemann Publishing Co., Oxford, 2003.

[28]. J. G. Sevillano, Scr. Mater. 49 (2003) 913-916

[29]. J. W. Cahn, Acta Metall. 11 (1963) 1275-1281.

[30]. R. Lagneborg, Acta Metall. 15 (1967) 1737-1745.

Tables

Table 1. Mechanical properties of PM 2000 aged at 475 ºC as a function of time.

	0 h	100 h	320 h	520 h
Young's Modulus (GPa)	168±9	---	183±8	190±8
Yield Strength (MPa)	744	951	998	1066
Tensile Strength (MPa)	913	1067	1079	1147
Elongation (L_o=5d_o) %	23.5	19	16	12
Area Reduction (%)	70	62	68.2	62.4

Figures

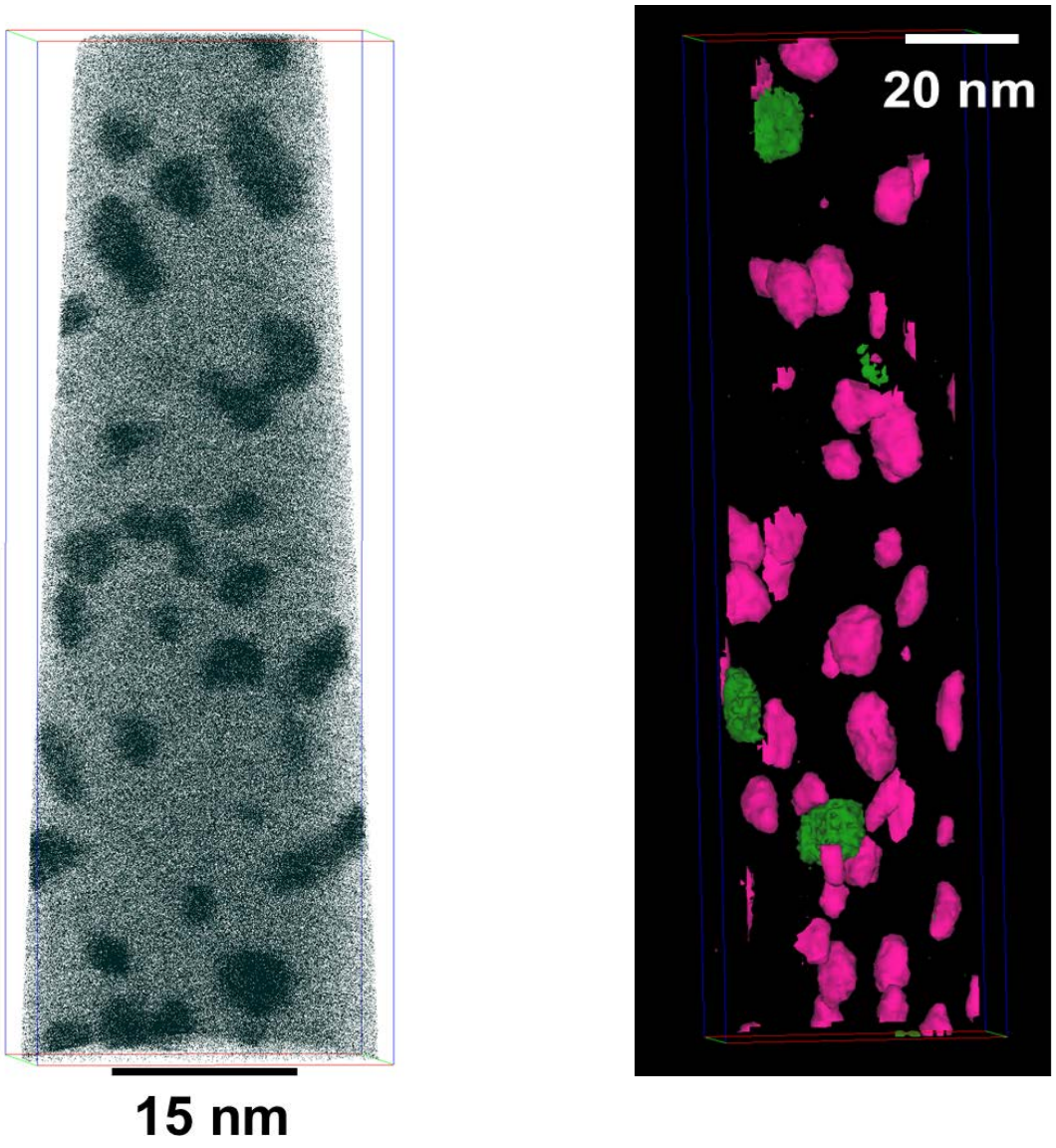

(a) (b)

Figure 1. (a) Atom distribution in PM 2000™ after ageing for 2000 h at 475 °C, and (b) 50% Cr (purple) and 5% Ti (green) isoconcentration surfaces after ageing for 3600 h at 435 °C.

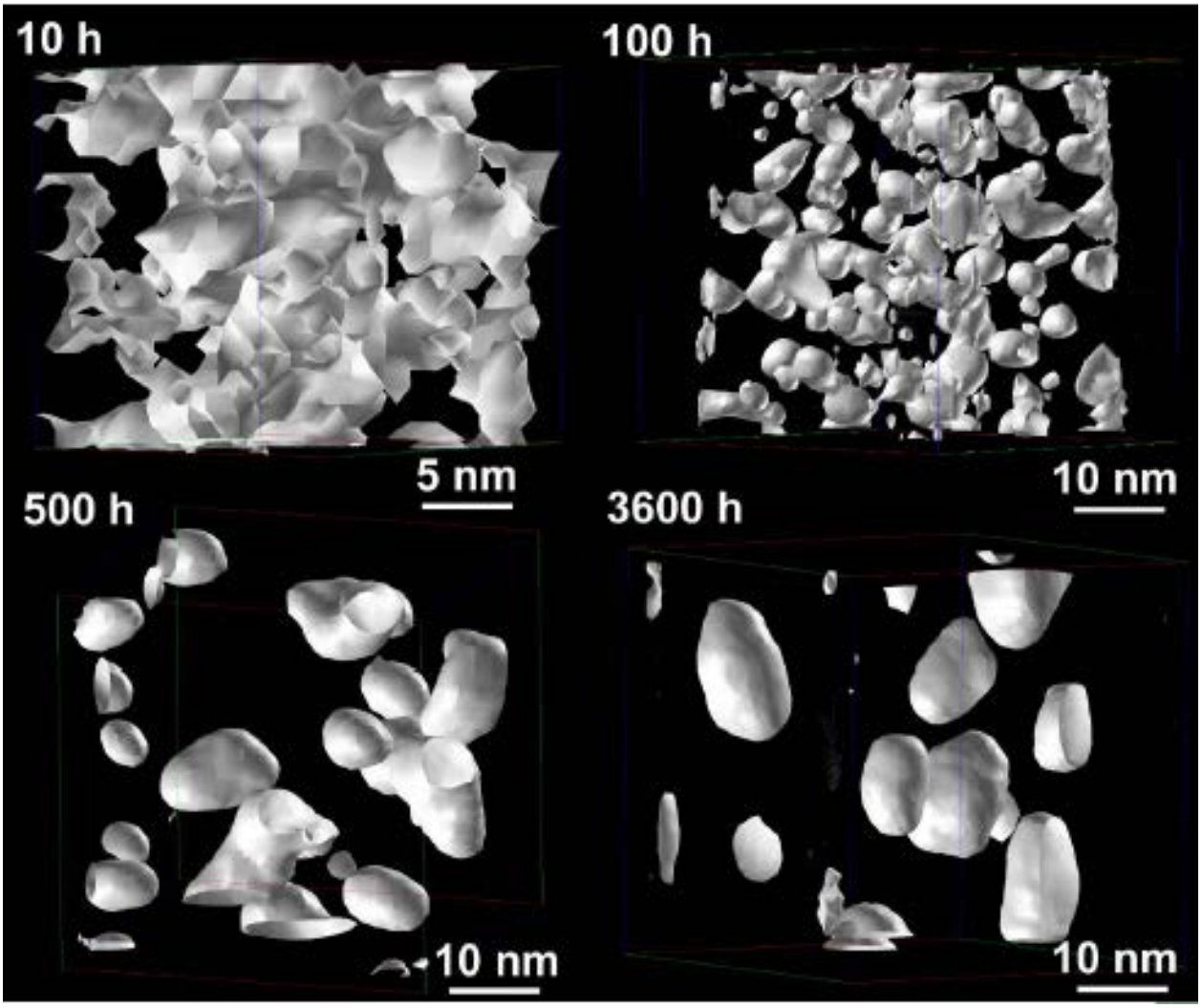

Figure 2. 30% Cr isoconcentration surface illustrating the three-dimensional microstructure after ageing at 475 °C for times ranging from 10 to 3600 h.

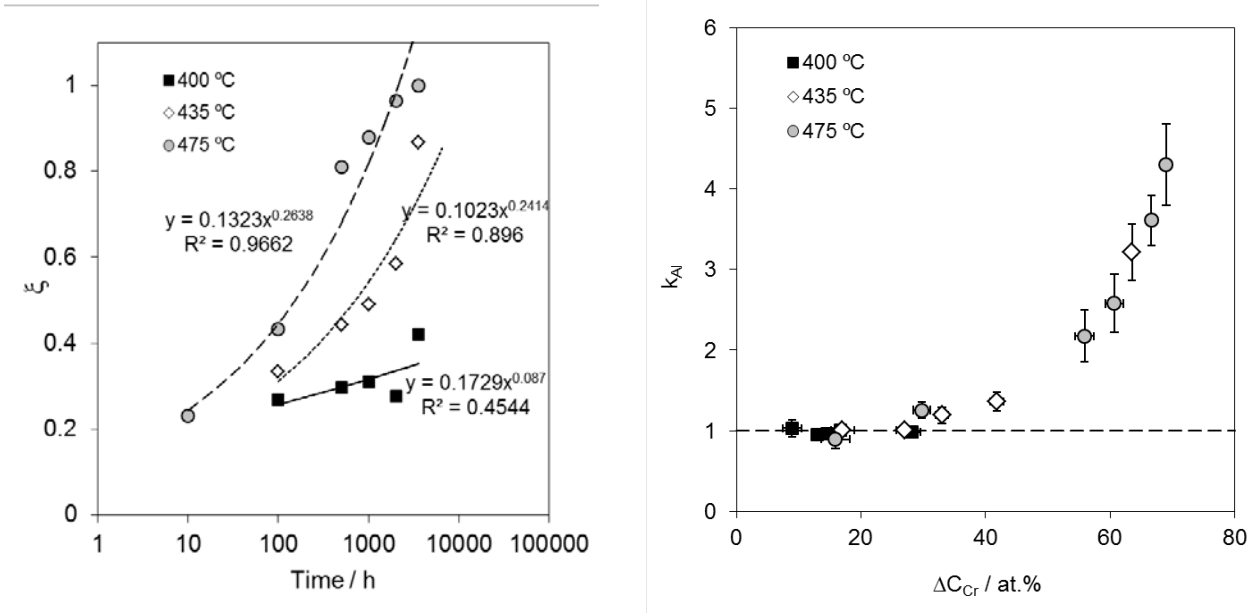

(a) (b)

Figure 3. The α-α′ phase separation during ageing at 400, 435 and 475 °C: (a) ξ evolution with ageing time and (b) evolution of Al-partitioning coefficient (k_{Al}) with the composition amplitude (ΔC_{Cr}) of α-α′ phase separation.

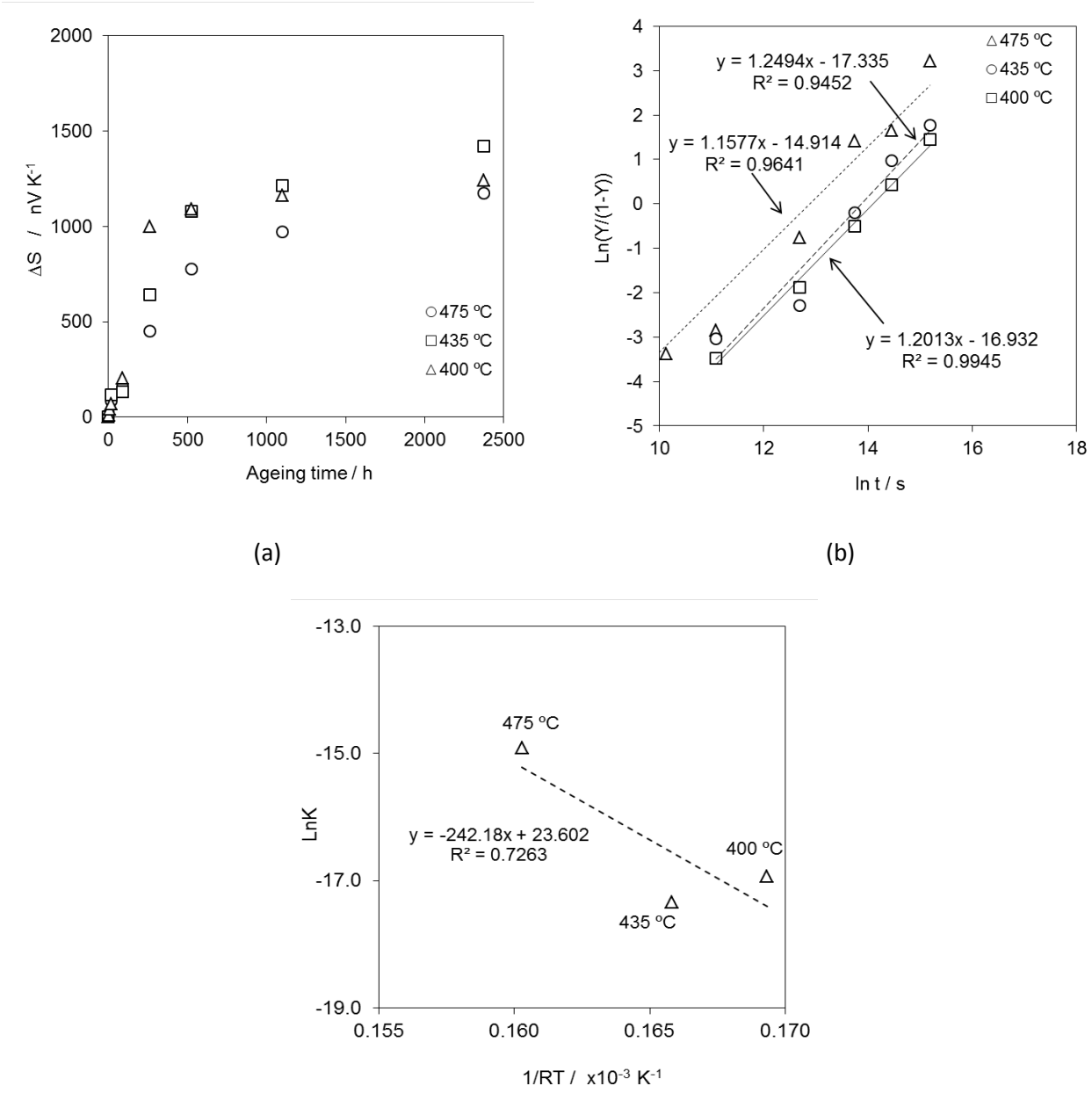

Figure 4. TEP analysis of α-α' phase separation: (a) TEP data measured at 400, 435 and 475 °C, (b) ln [Y/(1-Y)] as a function of ageing time, and (c) LnK vs 1/T plot derived from Austin-Rickett equation. Correlation factor R^2 is shown.

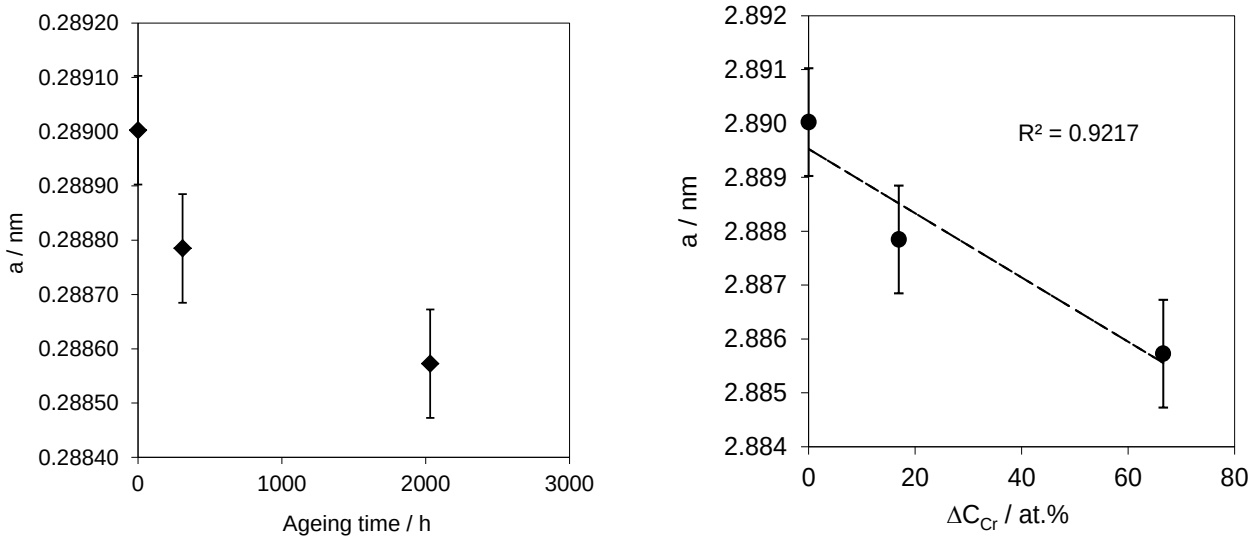

(a) (b)

Figure 5. Evolution of ferrite lattice parameter in PM2000^{TM} as a function of (a) ageing time at 475 °C, and (b) compositional amplitude (ΔC_{Cr})

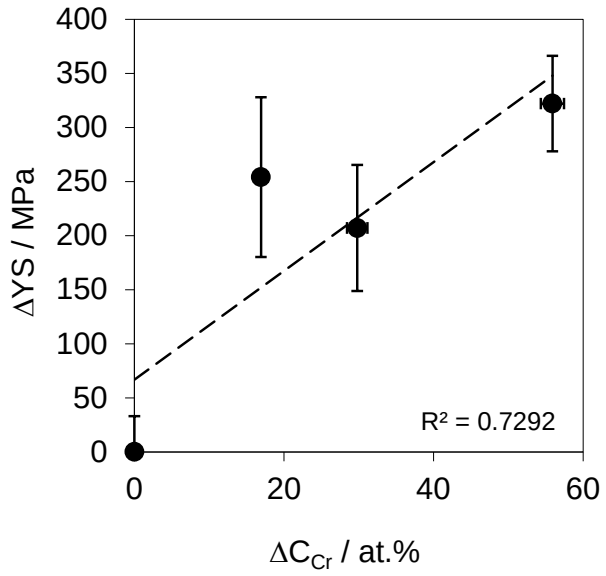

Figure 6. Evolution of the incremental change in yield strength with compositional amplitude. ΔC_{Cr} is the compositional amplitude and ΔYS is incremental change in yield strength.